

Turbulent diffusion and transport from a CO₂ lake in the deep ocean

Peter M. Haugan

Geophysical Institute, University of Bergen, Bergen, Norway

Guttorm Alendal

Bergen Center for Computational Science, University of Bergen, Bergen, Norway

Received 9 July 2004; revised 21 March 2005; accepted 14 April 2005; published 21 September 2005.

[1] If liquid CO₂ is stored as a dense “lake” on the deep ocean floor, it is expected to dissolve in seawater. Ocean currents and turbulence can increase the net rate of CO₂ release by several orders of magnitude compared to molecular diffusion. However, density stratification in the seawater created by dissolved CO₂ will tend to reduce vertical mixing. A two-dimensional numerical study with a high-resolution advection-diffusion model, coupled with a general turbulence model, reveals significant modifications of the boundary layer structure above a generic CO₂ lake taken to be 500 m in length and placed in a 10 km domain that is subject to specified far-field currents in the range of 0.05–0.20 m s⁻¹. Dissolution rates of order 0.07 μmol cm⁻² s⁻¹, reaching approximately 0.5 μmol cm⁻² s⁻¹ during a benthic storm, are predicted. The friction velocity is reduced above the CO₂ lake, and CO₂ concentrations corresponding to excess water densities of up to 0.5 kg m⁻³ occur in the lower 10 m of the water column. The persistency of this low-pH, CO₂-enriched water layer in weakly stratified and neutral background conditions in the model suggests that gravity current dynamics are important over considerable distances and should be considered in future larger-scale models and impact studies.

Citation: Haugan, P. M., and G. Alendal (2005), Turbulent diffusion and transport from a CO₂ lake in the deep ocean, *J. Geophys. Res.*, 110, C09S14, doi:10.1029/2004JC002583.

1. Introduction

[2] The increasing atmospheric CO₂ levels are a cause for concern among scientists, policy makers and the public at large. Impacts of elevated atmospheric CO₂ include not only global atmospheric warming but also acidification of ocean waters [Haugan and Drange, 1996; Caldeira and Wickett, 2003] measurable as reduced pH. On the basis of these projected consequences, Harvey [2004] has argued that the text of the Kyoto protocol of the legally binding United Nations Framework Convention on Climate Change implies a commitment to stabilize atmospheric CO₂ at 350–450 ppmv. This would require massive changes of the world energy infrastructure during this century [Caldeira *et al.*, 2003].

[3] Capture, transport and deep ocean storage of CO₂ is one option that might be considered to reduce the burden on the atmosphere and the near surface ocean, if its environmental impact in the deep sea is acceptable. Various techniques to dispose of CO₂ in the ocean have been described, including ship-based sprinkling from towed pipes, release of buoyant droplets of liquid CO₂ from bottom-mounted pipelines, and placement of pure liquid

CO₂ directly at the deep ocean floor. The Intergovernmental Panel on Climate Change has recently started work on a Special Report on Carbon Dioxide Capture and Storage [Intergovernmental Panel on Climate Change, 2002] (available at http://arch.rivm.nl/env/int/ipcc/pages_media/ccs-report.html) reviewing scientific, technical and economic aspects of both direct ocean storage and geological storage.

[4] The present paper focuses on processes that would affect placement of pure CO₂ directly at the deep ocean floor, i.e., a CO₂ lake. Fer and Haugan [2003] recently reviewed relevant physical and chemical processes and properties for this option and performed a model study of dissolution from a CO₂ lake at 3000 m depth. By coupling an analytic representation of velocity profiles and diffusivities in the turbulent boundary layer with a two-dimensional numerical advection and diffusion solver, they obtained estimates of net dissolution rates. The dissolution rate in realistic cases was found to be much higher than if controlled by molecular diffusion (0.0044 m yr⁻¹ [Ohsumi, 1997]) and critically dependent on externally specified current speeds. Fer and Haugan [2003] obtained an order of magnitude increase in CO₂ dissolution rate (0.1–1.6 m yr⁻¹) when increasing the speed from a typical deep sea current speed of 0.05 m s⁻¹ to a benthic storm case of 0.20 m s⁻¹. A key factor limiting dissolution was the development of density stratification in the water column

due to the elevated carbon concentration above and downstream of the lake.

[5] Here we present a new model study with numerically resolved boundary layer turbulence. The buildup, advection and diffusion of dissolved carbon is affected by shear production of turbulent kinetic energy in variable stratification. Our objective is to understand the interactions between these processes and their effect on the dissolution rate which turns out to be controlled primarily by the friction velocity. In order to address this coupled problem we have constructed a new process-oriented model based on freely available turbulence modules. In addition to imposed external velocity, we also studied the effects due to background density (salinity) stratification and internal wave activity. Key output parameters in addition to net dissolution rate and profiles of velocity and excess density near the lake, are the vertical extent, structure and pH (carbon concentration) of the developing boundary layer flowing away from the disposal site. These parameters are potentially important both for benthic biological impact as well as further mixing in the water column and ultimately retention time in the ocean.

[6] *Nakashiki* [1997] gave an overview of lake type storage concepts and pointed to the potentially important role of hydrodynamic instability and factors affecting turbulent diffusivities. *Kobayashi* [2003] recently performed a numerical study of a deep sea CO₂ lake including variable bottom topography and different, but fixed eddy diffusivities in a benthic boundary layer and the free stream above. Apart from these studies, several laboratory studies of fundamental CO₂ and hydrate properties, and ongoing small-scale deep sea experiments (P. Brewer, Monterey Bay Aquarium Research Institute, personal communication, 2004), we are unaware of other studies focusing on the dynamics of this sequestration option. For further background and review of other relevant papers, the reader is referred to the more extensive discussion by *Fer and Haugan* [2003].

[7] The following section describes the model setup including choice of turbulence model, solution strategy and initialization. Numerical results are presented in section 3 and some concluding remarks are given in section 4.

2. Model Configuration

[8] The simulations use the 1-D water column General Ocean Turbulence Model (GOTM) developed by *Burchard et al.* [1999] as the core solver. The model, with source code, is freely available at gotm.net and the users can choose between a number of standard turbulence parameterizations.

[9] Since GOTM only has transport equations for temperature and salinity included, a third tracer was included, the carbon concentration. This tracer is also dynamically active through increase in density for increasing carbon concentration. The international equation of state [United Nations Educational, Scientific, and Cultural Organization, 1981] was extended to take into account the effect that the enhanced concentration of dissolved inorganic carbon has on seawater density:

$$\rho_{\text{mix}} = \rho(S, T, p) + [M_{\text{CO}_2} - \rho(S, T, p)v_{\text{CO}_2}]C_T. \quad (1)$$

Here $\rho(S, T, p)$ (kg m⁻³) is the seawater density according to the standard equation of state and $v_{\text{CO}_2} = 34 \times 10^{-6} \text{ m}^3 \text{ mol}^{-1}$ is a conservative (high) estimate of the molar volume of CO₂. $M_{\text{CO}_2} = 44.01 \times 10^{-3} \text{ kg mol}^{-1}$ is the molar mass of CO₂. For the pressure range considered here, v_{CO_2} can be treated as constant. In equation (1) the heat release from the dissolution process has been neglected [*Haugan and Drange*, 1992].

[10] The tracer equation added to the source code follows the treatment of salinity. The equation solved by GOTM is

$$\frac{\partial}{\partial t} C = \frac{\partial}{\partial z} \left[(v'_t + \nu^C) \frac{\partial}{\partial z} C \right] + \Delta_x C + J_{\text{CO}_2}, \quad (2)$$

where C (mol m⁻³) is the carbon concentration and $\nu^C = 1.8 \times 10^{-9} \text{ m}^2 \text{ s}^{-1}$ is the molecular diffusivity for CO₂. The turbulent diffusivity, denoted v'_t (m² s⁻¹), will be discussed in section 2.1. The two last terms on the right hand side are, respectively, the horizontal tendencies and source term, to be discussed later.

[11] In a similar manner the horizontal momentum equation reads

$$\frac{du}{dt} = \int_z^0 \frac{\partial b}{\partial x} dz' + \frac{\partial}{\partial z} \left((\nu_t + \nu) \frac{\partial u}{\partial z} \right), \quad (3)$$

where u (m s⁻¹) is the horizontal velocity, $b = -g(\rho - \rho_0)/\rho_0$ (m s⁻²) is the buoyancy, and ρ_0 (kg m⁻³) is characteristic density of seawater. The molecular viscosity is $\nu = 1.8 \times 10^{-9} \text{ (m}^2 \text{ s}^{-1}\text{)}$, while the turbulent viscosity is denoted ν_t (m² s⁻¹). The “internal pressure” term, first on the right hand side, has been used to provide horizontal tendencies for the momentum equation.

2.1. Choice of Turbulence Model

[12] The turbulent viscosity and diffusivity are functions of the turbulent kinetic energy, k (m² s⁻²), and a length scale, l (m):

$$\nu_t = c_\mu k^{\frac{1}{2}} l \quad \nu'_t = c'_\mu k^{\frac{1}{2}} l, \quad (4)$$

with the dimensionless stability functions c_μ and c'_μ . GOTM provides different options for calculating the turbulent kinetic energy, length scale, and related stability functions.

[13] Since the dissolved carbon will alter the stratification of the seawater column it is important to choose a turbulence model developed for stratified environments. Strong stratification will suppress turbulence, hence reduce the turbulent viscosity and diffusivity. As the stratification increases, the vertical scale of turbulent eddies decreases until they are not taking part in the energy cascade but loose their energy through radiating internal waves [*Kantha and Clayson*, 2000].

[14] The simulations presented here use a “one-equation” model, i.e., the turbulent kinetic energy is calculated from a differential transport equation while the turbulent length scale and the stability functions are calculated from empirical relations.

Table 1. Labels of the Different Simulations^a

Simulation	Background Velocity, m/s	Stratification	Internal Waves
U05NIW	0.05	no	yes
U05SIW	0.05	yes	yes
U10NIW	0.1	no	yes
U10SIW	0.1	yes	yes
U20NIW	0.2	no	yes
U20SIW	0.2	yes	yes
U05N	0.05	no	no
U05S	0.05	yes	no
U10N	0.1	no	no
U10S	0.1	yes	no
U20N	0.2	no	no
U20S	0.2	yes	no

^aThe background stratification enforced on the cases labeled “S” corresponds to a linear increase in salinity from 30.00 to 35.01 over the deepest 100 m. The label “IW” indicates use of the internal wave model.

[15] For the length scale the ISPRAMIX model [Eifler and Schrimpf, 1992] is used. Close to the bottom l is obtained from the formula

$$l = \frac{\kappa \tilde{z}}{1 + \frac{\kappa \tilde{z}}{c_2 h_m}} (1 - R_f), \quad (5)$$

where \tilde{z} is the distance from the bottom and κ is the von Kármán constant. The fraction in (5) gives a linear behavior of l near boundaries and a value proportional to the thickness of the mixed layer h_m , i.e., the distance from the bottom having a turbulent kinetic energy less than the threshold value of 10^{-5} . Further away from the interface, $l = c_2 h_m$, where $c_2 = 0.065$ based on experimental data. The factor $(1 - R_f)$, accounts for the effect of stratification on the length scale. The flux Richardson number is the fraction between buoyant production, B , and shear production P ; $R_f = -B/P$.

[16] The ISPRAMIX ocean model [Eifler and Schrimpf, 1992] is also used for stability functions:

$$c_\mu = \text{const} = 0.5 \quad (6)$$

$$c'_\mu = c_\mu \frac{1}{P_r^0} (1 - R_f)^{1/2}, \quad (7)$$

with the neutral Prandtl number $P_r^0 = 0.7143$.

[17] When there is suppression or extinction of turbulence [Kantha and Clayson, 1994] (diagnosed by $k < k_{\text{lim}}$, set to the standard GOTM value of 10^{-6}), an option for transfer of energy to internal waves has been used. In this case, eddy viscosity and diffusivity ν_t and ν'_t are set to empirical values typical in the presence of internal wave activity (IW) and shear instability (ShI). This model is described by

$$\nu_t = \nu_t^{\text{IW}} + \nu_t^{\text{ShI}} \quad \nu'_t = \nu_t^{\text{IW}} + \nu_t^{\text{ShI}}, \quad (8)$$

where

$$\nu_t^{\text{IW}} = 10^{-4} \quad \nu_t^{\text{ShI}} = 5 \cdot 10^{-5}. \quad (9)$$

The “ShI” parts are functions of the Richardson number according to

$$\nu_t^{\text{ShI}} = \nu_t^{\text{ShI}} = \begin{cases} 0 & R_i > 0.7 \\ 5 \cdot 10^{-3} \left(1 - \left(\frac{R_i}{0.7} \right)^2 \right)^3 & 0 < R_i < 0.7, \\ 5 \cdot 10^{-3} & R_i < 0 \end{cases} \quad (10)$$

with the gradient Richardson number

$$R_i = N^2/M^2. \quad (11)$$

N (s^{-1}) and M (s^{-1}) are, respectively the buoyancy frequency and the shear frequency. The unit of all diffusivities is $\text{m}^2 \text{s}^{-1}$. The IW and ShI contributions are always used together according to equation (8). For simplicity we hereafter refer to this as the internal wave (IW) model.

2.2. Solution Strategy and Initialization

[18] Since the GOTM is a one dimensional column model we incorporated it into a two-dimensional (2-D) wrapper. The wrapper keeps copies of the arrays in GOTM. Each time step consist of copying vertical columns from the wrapper into GOTM, updating the turbulence fields, performing a time step for the water column, and updating the wrapper copy. Horizontal advection and diffusion is submitted to GOTM through the horizontal tendency term in equation (2) and the internal pressure in equation (3). Hence GOTM does the actual time stepping.

[19] In all the numerical experiments the lake is assumed to be at 3000 m depth. The vertical grid is focused at the bottom with smallest $\Delta z \sim 0.23$ m. The lake is assumed to be 500 m long, with center at $x = 2500$ m along an axis extending to 10,000 m. In the same manner the grid is focused over the position of the lake, smallest $\Delta x \sim 19$ m and largest $\Delta x \sim 185$ m.

[20] Each of the simulations is initiated with a prescribed homogeneous flow field throughout the domain. The lateral boundary conditions for velocity are of Dirichlet type with the same prescribed velocity. Before the source of CO₂ becomes active, the model is integrated forward in time for 3 hours to assure development of the turbulent boundary layer. Neuman boundary conditions, i.e., zero gradient at the boundaries, is used for the carbon concentration.

[21] The source term in equation (2) is a simplified version of the flux used by Fer and Haugan [2003]:

$$J_{\text{CO}_2} = \frac{1}{1 - \tilde{C}_s} \left[K_m \frac{\rho_s}{M_S} (\tilde{C}_s - \tilde{C}_{\text{amb}}) \right], \quad (12)$$

where $\tilde{C}_s \sim 35 \times 10^{-3}$ is the solubility CO₂ of seawater (mole factor), \tilde{C}_{amb} the mole factor in the ambient water, and ρ_s (kg m^{-3}) is the density of saturated water. The molar mass of the CO₂ enriched seawater M_S (kg mol^{-1}) is

$$M_S = M_w (1 - \tilde{C}_s) + M_{\text{CO}_2} \tilde{C}_s, \quad (13)$$

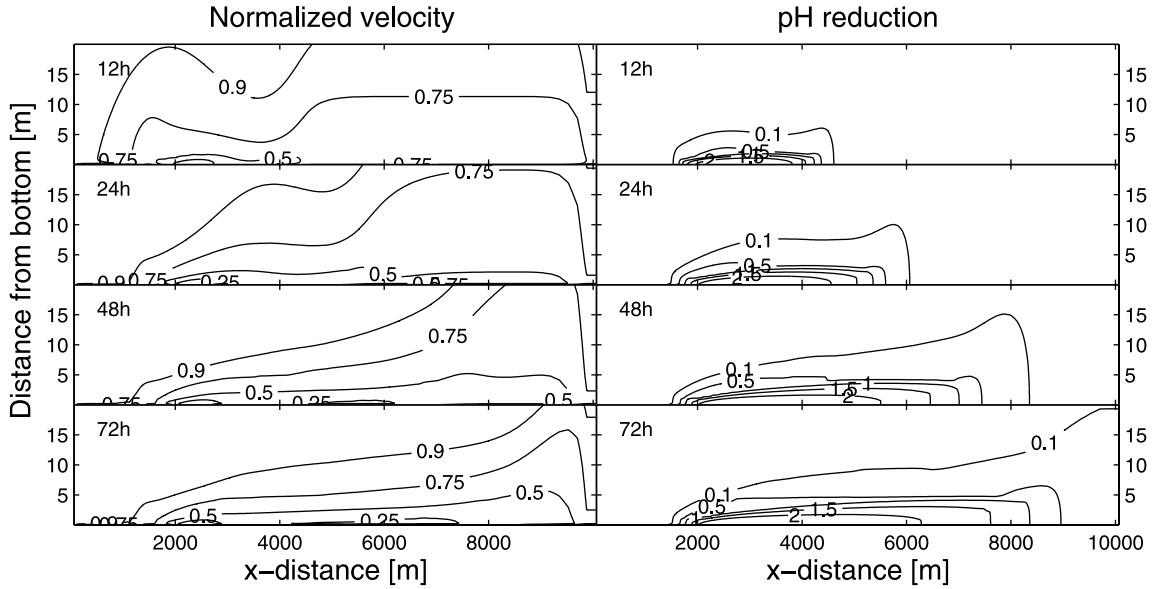


Figure 1. Time evolution of the case U05NIW. Normalized (left) u velocity and (right) pH reduction. The current moves in positive x direction, and the lake is 500 m wide with center at $x = 2500$ m.

and the mass transfer K_m (m s^{-1}) equal to

$$K_m = 0.1u_*Sc^{-0.67} \quad (14)$$

using a Schmidt number $Sc = \nu/D = 10^3$. The friction velocity u_* (m s^{-1}) is calculated by GOTM by updating the bottom roughness,

$$z_0^b = 0.1 \frac{\nu}{u_*^b} + 0.03h_0^b, \quad (15)$$

and using the law-of-the-wall relation for friction velocity:

$$u_*^b = \frac{\kappa}{\ln\left(\frac{0.5h_1 + z_0^b}{z_0^b}\right)} |u_1|, \quad (16)$$

where κ is the von Kármán constant, $h_0^b = 0.05$ m is a constant bottom roughness, and the index “1” indicates values at the center of the first grid box at the bottom. The two equations are solved through an iterative process.

3. Results

[22] Three different prescribed background currents have been simulated, $u = 5 \text{ cm s}^{-1}$, 10 cm s^{-1} , and 20 cm s^{-1} . Each of the cases has also been performed both without background stratification and with a prescribed salinity gradient of $\Delta S = 0.01$ over the deepest 100m. Furthermore, additional simulations were made without the IW model included. The different cases and labels used on them are given in Table 1.

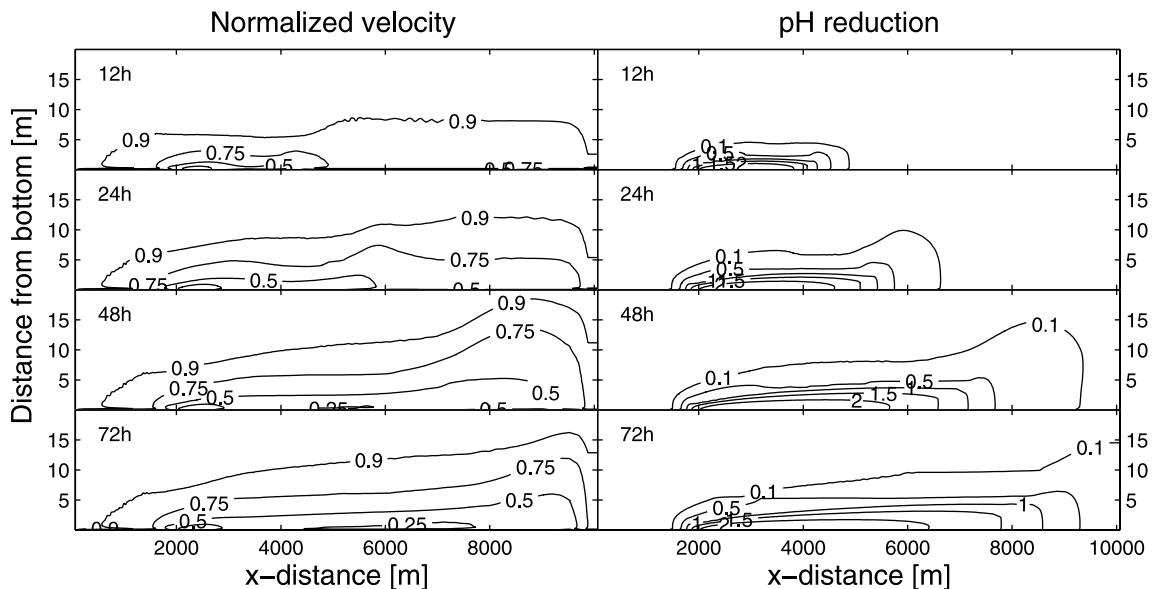


Figure 2. Time evolution of the case U05SIW. Normalized (left) u velocity and (right) pH reduction. The current moves in positive x direction, and the lake is 500 m wide with center at $x = 2500$ m.

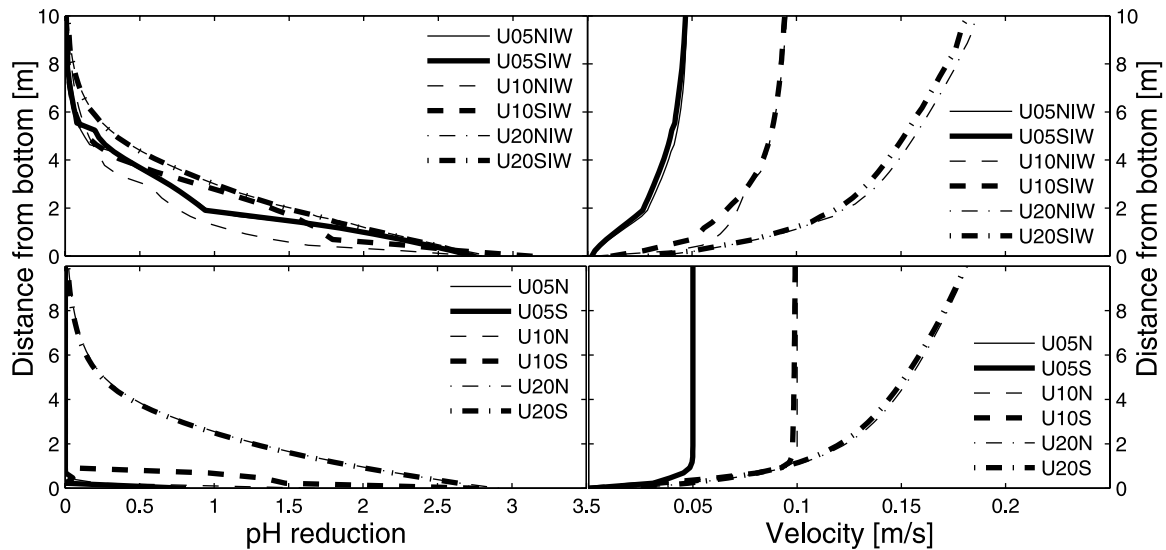


Figure 3. (left) Reduction in pH and (right) velocity profiles for the different simulations at $x = 2500$ m after 72 hours. Upper figures show results with the internal wave model included, while in the lower figures this effect has been excluded.

[23] Figure 1 shows time evolution of the case U05NIW, hence a background current of 5 cm/s, no stratification, and with the internal wave model included. The boundary layer is sharpened as the stratification is increased due to the dissolution of CO₂. The vertical extent of reduced pH stays below approximately 5 m. When the background stratification is included (Figure 2) the boundary layer is thinner in the unperturbed situation, i.e., far downstream. The end situation looks similar both for the velocity and the pH fields.

[24] Vertical profiles of pH reduction and horizontal velocity at the center of the “lake” are shown in Figure 3. The reduced pH profiles show the impact from the internal wave model on vertical mixing. Except for high-velocity situations, the pH reduction remains within 1 m above the sea floor in the absence of internal wave mixing. Mixing

due to internal waves distributes the carbon, hence the pH reduction, over a larger vertical area.

[25] The right panels in Figure 3 show that when the IW model is in use (Figure 3 (top)), there is a distinct difference in the velocity profile at the bottom. Notice that the U10NIW profile follows closer to the U20 profiles than the similar profile with background stratification (U10SIW). On the other hand, when the IW activity is turned off, the profiles are more equal for the first 0.5 m above the bottom. This indicates that the case with background velocity set to 10 cm/s, and with IW activity, is most influenced by the enforced background stratification.

[26] The friction velocity controls the flux rate of CO₂ from the lake through equations (12) and (14). Figure 4

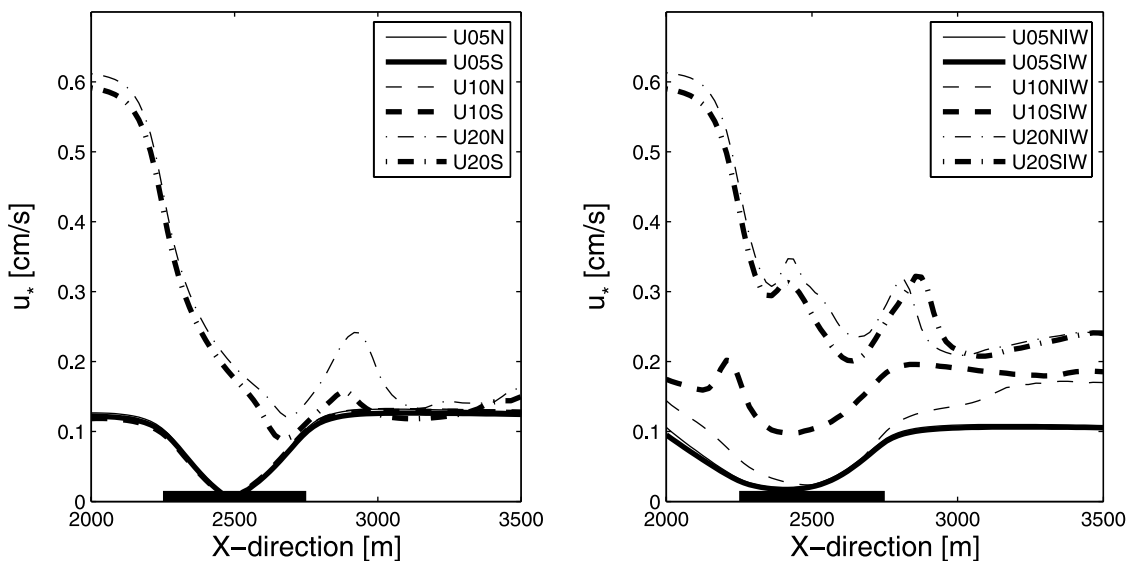


Figure 4. Friction velocity (left) without and (right) with the internal waves model. The position of the lake is between $x = 2250$ and $x = 2750$.

Table 2. Mean Dissolution Rates Over the CO₂ Lake

Simulation	u_* , cm/s	Influx, $\mu\text{mol}/\text{cm}^2 \text{ s}$	Dissolution Rate, cm/yr
U05NIW	0.04	0.06	59
U05SIW	0.04	0.05	55
U10NIW	0.05	0.07	69
U10SIW	0.13	0.19	193
U20NIW	0.31	0.46	468
U20SIW	0.28	0.42	421
U05N	0.05	0.07	66
U05S	0.05	0.06	58
U10N	0.05	0.06	64
U10S	0.05	0.06	57
U20N	0.23	0.34	340
U20S	0.20	0.30	303
U20 stratified	0.22	0.30	296
U20 unstratified	0.25	0.35	355
U10 stratified	0.13	0.19	187
U10 unstratified	0.11	0.17	165
U05 stratified	0.02	0.03	34
U05 unstratified	0.03	0.04	42

shows the computed friction velocity without IW (Figure 4 (left)) and with IW (Figure 4 (right)). Without IW the friction velocities are almost identical for U05 and U10 cases. This is consistent with almost identical near bottom linear velocity profiles for the U05 and U10 in Figure 3. The U20 case has much higher velocities near the sea floor. The drop in friction velocity on top of the CO₂ lake must be caused by enhanced stratification due to increased CO₂ concentration.

[27] When the IW model is included, the friction velocity on top of the lake increases for all cases, with a special increase in friction velocity for the U10SIW case.

[28] The difference in friction velocity shown in Figure 4 leads to different dissolution rates of CO₂ from the lake. Table 2 shows the mean flux of CO₂ through the CO₂-seawater interface after reaching steady state. The fluxes are all within the rates measured in experiments (see *Fer*

and Haugan [2003] for a review). Decreasing mean flow reduces the flux. As expected, high velocity increases the dissolution rates. As discussed above, the cases with $U = 10 \text{ cm s}^{-1}$ under influence from IW show remarkably different behavior. Without background stratification, the numbers are comparable with the $U = 5 \text{ cm s}^{-1}$ cases. With background stratification, the dissolution rates are between the low- and high-velocity situations. Without the IW, the $U = 10 \text{ cm s}^{-1}$ cases are both similar to the $U = 5 \text{ cm s}^{-1}$ cases, hence indicating that the current is not strong enough to create enough turbulent energy for enhanced mixing. However, with the inclusion of stratification the extra mechanism for mixing from IW “kicks in” and produces the extra mixing. All cases, except for the U10NIW and U10SIW cases, indicate reduced mixing with ambient background stratification.

[29] In Figure 5 the vertical distribution of the dissolved CO₂, normalized against total amount of excess CO₂ in the water column, and pH reduction at $x = 7500 \text{ m}$ after 3 days are shown. It only shows the profiles for the IW cases. Without the IW, all the CO₂, except for the cases with high velocity, stay within the first meter above the seafloor. Notice the relatively high concentration of CO₂ near the sea bottom for the U10SIW case. The non stratified counterpart U10NIW follows the U20NIW case. The reason for this discrepancy follows from the high friction velocity for U10SIW (Figure 4). Hence that case has a larger flux of CO₂ and higher stratification downstream. The vertical diffusion is therefore reduced and the CO₂ enriched water stays focused at the seafloor. Even if the flux is higher for the U20SIW and U20NIW cases, the background velocity is strong enough to produce mixing. Hence the CO₂ is distributed over a larger vertical volume. Even though the U10NIW follows the relative vertical distribution of CO₂ for the high-velocity cases, there is less CO₂ in the water column. This can be seen in the right panel of

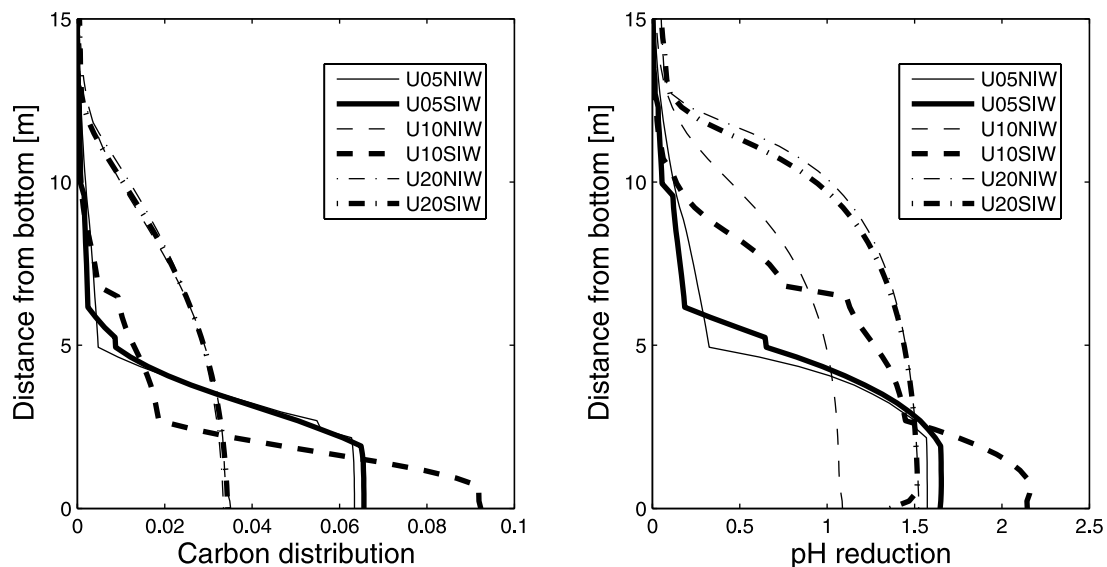


Figure 5. Normalized vertical distribution of (left) CO₂ and (right) pH reduction at $x = 7500 \text{ m}$ after 3 days.

Figure 5, showing the reduction in pH as an exponential image of the excess CO₂ concentration.

4. Conclusion

[30] The results shown here originate from a simple 2-D expansion of the vertical General Ocean Turbulence Model. It is shown that the increase in density caused by the enhanced CO₂ concentration alters the turbulence in the bottom boundary layer. This reveals the importance of using proper turbulence closure models capable of describing large density gradients.

[31] We have demonstrated that internal waves generate mixing that is crucial for the vertical spreading of dissolved CO₂. The implementation of IW in the model is most likely sensitive to the threshold limit enforced, i.e., turbulent kinetic energy below 10⁻⁶ triggers the IW viscosities in equation (8). Changing this threshold may change the velocity and stratification at which there is a transition from slow to rapid dissolution from a CO₂ lake, as indicated in Table 2.

[32] The two dimensional wrapper used in this study includes very basic advection routines. As seen in Figure 5, there will be a density increase that may generate a horizontally propagating buoyant plume. The present simulation tool is not fully capable of describing such an event. Even more important might be the lack of vertical velocity component. Vertical advection would be expected to play a role in situations where incoming water meets water with high CO₂ concentrations above the lake. Vertical advection would also play a role in cases of unstable stratification, as seen close to the bottom for the U20SIW case in right panel of Figure 5. Hence the next natural step will be to include GOTM in a full nonhydrostatic Computational Fluid Dynamics solver. Such a model would include the IW mechanism and remove the need for the empirical IW parameters as used here.

[33] **Acknowledgment.** This work has been funded by New Energy Development Organization (NEDO) of Japan.

References

- Burchard, H., K. Bolding, and M. R. Villarreal (1999), GOTM—A general ocean turbulence model: Theory, applications and test cases, *Tech. Rep. EUR 18745 EN*, CEC Joint Res. Cent., Ispra, Italy.
- Caldeira, K., and M. E. Wickett (2003), Anthropogenic carbon and ocean pH, *Nature*, 425, 365.
- Caldeira, K., A. K. Jain, and M. I. Hoffert (2003), Climate sensitivity uncertainty and the need for energy without CO₂ emission, *Science*, 299, 2052–2054.
- Eifler, W., and W. Schrimpf (1992), ISPRAMIX, a hydrodynamic program for computing regional sea circulation patterns and transfer processes, *Tech. Rep. EUR 14856 EN*, CEC Joint Res. Cent., Ispra, Italy.
- Fer, I., and P. M. Haugan (2003), Dissolution from a liquid CO₂ lake disposed in the deep ocean, *Limnol. Oceanogr.*, 48, 872–883.
- Harvey, L. D. D. (2004), Declining temporal effectiveness of carbon sequestration: Implications for compliance with the United Nations framework convention on climate change, *Clim. Change*, 63, 259–290.
- Haugan, P. M., and H. Drange (1992), Sequestration of CO₂ in the deep ocean by shallow injection, *Nature*, 357, 318–320.
- Haugan, P. M., and H. Drange (1996), Effects of CO₂ on the ocean environment, *Energy Convers. Manage.*, 37, 1019–1022.
- Intergovernmental Panel on Climate Change (2002), *Proceedings of the Workshop on Carbon Dioxide Capture and Storage*, Energy Res. Cent. for the Netherlands, Regina, Canada.
- Kantha, L. H., and C. A. Clayson (1994), An improved mixed layer model for geophysical applications, *J. Geophys. Res.*, 99, 25,235–25,266.
- Kantha, L. H., and C. A. Clayson (2000), *Small Scale Processes in Geophysical Fluid Flows*, *Int. Geophys. Ser.*, vol. 67, Elsevier, New York.
- Kobayashi, Y. (2003), Bfc analysis of flow dynamics and diffusion from the CO₂ storage in the actual sea bottom topography, *Trans. West Jpn. Soc. Nav. Archit.*, 106, 19–31.
- Nakashiki, N. (1997), Lake-type storage concepts for CO₂ disposal option, *Waste Manage.*, 17, 361–367.
- Ohsumi, T. (1997), CO₂ storage options in the deep-sea, *Mar. Technol. Soc. J.*, 29, 58–66.
- United Nations Educational, Scientific, and Cultural Organization (1981), Tenth report of the joint panel on oceanographic tables and standards, *UNESCO Tech. Pap. Mar. Sci.*, 36, 25 pp.

G. Alendal, Bergen Center for Computational Science, University of Bergen, Thormøhlensgt. 55, N-5008 Bergen, Norway. (guttorm.alendal@bccs.uib.no)

P. M. Haugan, Geophysical Institute, University of Bergen, Allegaten 70, N-5007 Bergen, Norway. (peter.haugan@gfi.uib.no)